ELSEVIER

Journal of Neuroscience Methods 94 (1999) 27–40

JOURNAL OF NEUROSCIENCE METHODS

www.elsevier.com/locate/jneumeth

Simultaneous multi-site recordings and iontophoretic drug and dye applications along the trigeminal system of anesthetized rats

Sebastian Haidarliu *, Ronen Sosnik, Ehud Ahissar

Department of Neurobiology, The Weizmann Institute of Science, Rehovot 76100, Israel

Received 12 June 1999; accepted 30 July 1999

Abstract

A multi-electrode system that permits simultaneous recordings from multiple neurons and iontophoretic applications at two or three different brain sites during acute experiments is described. This system consists of two or three microdrive terminals, each of which includes four electrodes that can be moved independently and used for both extracellular recordings and microiontophoretic drug administration. Drug applications were performed during standard extracellular recordings of multiple single-units via specialized combined electrodes (CEs), which enable ejection of neuroactive substances and recording of neuronal activity from the same electrode. With this system, we were able to successfully record simultaneously from different levels (brainstem, thalamus, and cortex) of the vibrissal ascending pathway of the anesthetized rat. Herein, examples of simultaneous recordings from the brainstem and thalamus and from the thalamus and cortex are presented. An effect of iontophoretic applications of agonists and antagonists of metabotropic glutamate receptors (mGluRs) in the thalamus is demonstrated, and the extent of drug diffusion in the barrel cortex is demonstrated with biocytin. This new multi-electrode system will facilitate the study of transformations of sensory information acquired by the whiskers into cortical representations.

Keywords: Barrel cortex; Brainstem trigeminal nuclei; Microiontophoresis; Multi-electrode array; Multi-site recordings; Sensory systems; Thalamus; Vibrissal representation

1. Introduction

Early stages of the processing of sensory information typically involve the following structures: a specialized peripheral receptor apparatus, which encodes sensory information; intermediate structures, which are usually considered as relay stations; and primary cortical domains, which provide internal representations of the sensory information. One of the most structured mammalian ascending pathways is the rodent system that processes vibrissal touch. Whisking rodents utilize their vibrissae for active touch by moving them rhythmically around 8 Hz (Vincent, 1912; Welker, 1964; Carvell and Simons, 1990). The trigeminal pathway, which conveys vibrissal information, contains distinct topologically corresponding features at different levels (Van der Loos, 1979): barrelettes in trigeminal nuclei of the brainstem (Ma, 1991; see also Belford and Killackey, 1979; Arvidson, 1982; Ma and Woolsey, 1984), barreloids in the thalamus (Van der Loos, 1976; Land et al., 1995), and barrels in the postero-medial barrel sub-field (PMBSF) of the somatosensory cortex (Woolsey and Van der Loos, 1970). Investigation of the transformation (from sensory encoding to cortical representation) of tactile information requires simultaneous recordings from different levels of the ascending pathway.

Previously, we suggested that during tactile exploration, sensory information about the location and texture of external objects is processed by reciprocal interactions of thalamic and cortical neuronal populations that perform an active temporal decoding of information encoded at the periphery (Ahissar et al., 1997; Ahissar, 1998). In order to test this, and alternative models, simultaneous recordings from multiple neurons of the brainstem, thalamus, and somatosensory

* Corresponding author. Tel.: +972-8-9344321; fax: +972-8-9344140.

E-mail address: bnsebast@weizmann.ac.il (S. Haidarliu)

0165-0270/99/$ - see front matter
PII: S0165-0270(99)00123-5

cortex are crucial. Critical testing of the operation of the thalamocortical loop requires 'opening the loop,' which might be achieved by application of pharmacological modulators that reduce the coupling between the cortex and thalamus.

Many methods have been described for obtaining simultaneous recordings from multiple neurons in vivo. In 1971 a 'connector skull cap' was developed to which a large number of cortical, needle electrodes could be attached (Kloprogge, 1971). Later, a ten-wire electrode for multi-unit recordings, coupled with a miniature frequency modulated transmitter and designed for freely-moving animals, was developed (Eichenbaum et al., 1977). Further advances in electrode technology resulted in construction of multiple, floating electrodes for chronic implantation (Legendy et al., 1984), and of planar, multisite microprobes for cortical, extracellular multi-unit recordings (Drake et al., 1988). Sets of 30 microelectrodes, constructed from platinum/iridium wire and coated with quartz glass were developed (Kruger and Bach, 1981) and successfully used in electrophysiological experiments (Kruger and Aiple, 1988). Other varieties of electrode arrays, bundles, and constructions include arrays made from 8–11 teflon-insulated, platinum/iridium wires (Palmer, 1990); slim, needle-shaped, multi-wire microelectrodes composed of 12 insulated nichrome wires embedded in epoxylite resin (Jellema and Weijnen, 1991); nine electrodes, gathered into three bundles with three wires per bundle (Olds, 1991); two independent bundles that each contain eight 25 mm-long, Formwar-insulated nichrome wires (Wiener, 1993); and Utah Intracortical Electrode Arrays that consist of a 10×10 matrix of 100 needles (1.5 mm in length) with an inter-needle spacing of 0.4 mm, and are designed for single-unit and multi-unit recordings from the cortex (Nordhausen et al., 1994). Recently, Nicolelis et al. demonstrated the importance of simultaneous recording of the extracellular activity of large populations of single neurons distributed at different levels of the neuraxis (Nicolelis et al., 1995, 1997, 1999). In these experiments, bundles and arrays of 8–16 microwires were chronically implanted in different neuronal structures of the rat and monkey.

Unfortunately, electrodes that are arranged in arrays, bundles, or other monolithic structures have serious disadvantages: the recording elements of these devices cannot be independently-positioned in order to optimize the signal-to-noise ratio and receptive field characteristics, and cannot be shifted from one cortical layer to the other, because their position is determined by permanent fixation upon initial penetration. Therefore, electrode devices that permit independent movement of each of the electrodes in the device were developed. One example is a multi-electrode recording system that contains a 19-channel matrix drive with individually-controllable, fiber microelectrodes (Reitboeck and Werner, 1983). This system was later adapted for multiple recordings in the behaving monkey (Mountcastle et al., 1991). Another, more flexible multi-electrode recording system that includes six or eight independently-movable, glass-insulated, tungsten microelectrodes was developed by De Ribaupierre, and further adapted to the behaving monkey by Abeles and colleagues (Abeles et al., 1993; Vaadia et al., 1995; Ahissar et al., 1998; Prut et al., 1998) and to anesthetized cats, guinea pigs, and rats by Villa et al. (1999). The electrodes most frequently used for multiple single neuron recordings are extensively reviewed elsewhere (Schmidt, 1999).

Herein, a system for achieving simultaneous recordings with independently-movable electrodes and iontophoretic administration of drugs and neuronal markers at different brain sites is described. This system is an extension of our previously described, single site recording system (Haidarliu et al., 1995). Using our novel multiple-site recording system, we were able to record simultaneously from different sites along the ascending vibrissal pathway, to modulate neuronal function by iontophoresis of neuromodulatory compounds, and to stain neuronal tissues and single neurons using biocytin.

2. Methods

2.1. Microelectrodes, microdrive terminals, and microelectrode positioning systems

Each multi-electrode array contained four electrodes, of which, for the experiments described here, one or two were CEs, and the other two or three were regular tungsten-in-glass electrodes (TEs). The optimal parameters for producing CEs with relatively uniform characteristics, which requires electrode pulling such that electrode tips of approximately uniform shape and dimension are obtained, was determined. Previously, we showed that three types of tip profiles (items 14–16 in Fig. 1 of Haidarliu et al., 1995) can be obtained by manipulating the temperature and timing of magnet activation while pulling with a microelectrode vertical puller (PE-2; Narishige, Japan; Haidarliu et al., 1995). This procedure was simplified, and used herein, to obtain optimal tip profiles (item 16 in Fig. 1 of Haidarliu et al., 1995) for subsequent grinding as follows: (i) the magnet was deactivated; (ii) the necessary coil temperature was provided by maintaining the current between 14.3 and 14.5 A; (iii) the shaft length, which is the distance from the middle of the heating coil to the etched tip, was 70–75 mm when borosilicate glass capillaries with outer diameters of 1.2 mm, inner diameters of 0.69 mm, and lengths of 10 cm, and tungsten rods with diameters of 125 μm were used; (iv) the lower chuck was manually rotated about 360, instead of 180

degrees; and (v) 10 mm (not 6 mm) of the tungsten rod was etched.

For advancing electrodes into the brain tissue, we used a remotely-controlled Electrode Positioning System (Alpha Omega Engineering; Nazareth, Israel; Villa et al., 1999). For our new multi-site recording and iontophoresis system, we developed a simple and reliable microdrive terminal (Fig. 1), based on the terminal we previously developed (Haidarliu et al., 1995). All the components of this microdrive terminal (screw clamp for the control cable for iontophoresis, pin-mounting board, guide-holder, and the guiding and electrode-fixating tubes) were made of stainless steel or plexiglass, and were connected to a teflon fixture. Each microdrive terminal was attached to a micromanipulator by a stainless steel bar. The blunt ends of the electrodes were kinked and inserted into the guiding and electrode-fixating tubes, thus providing a strong mechanical connection and reliable electrical contact. The electrode guide, which contains four linearly-arranged pieces of polyimide tubing, insured that the initial and parallel positions of the electrodes (inter-electrode distances of 280 μm, which were determined by the outer diameter of the polyimide tubings) were maintained as the electrodes were advanced into the brain tissue. The control cable for iontophoresis and the silver wires emanating from the capillaries were easily and tightly attached to the microdrive terminal. The terminal was equipped with a special screw clamp and a miniature pin-mounting board. Into each capillary of the CEs, a teflon-insulated silver wire was inserted such that the tip of the wire was exposed. The opposite end of each silver wire was labeled with a piece of tape and soldered to a pin on the mounting board. This fixation prevented the silver wires from exiting from the capillaries.

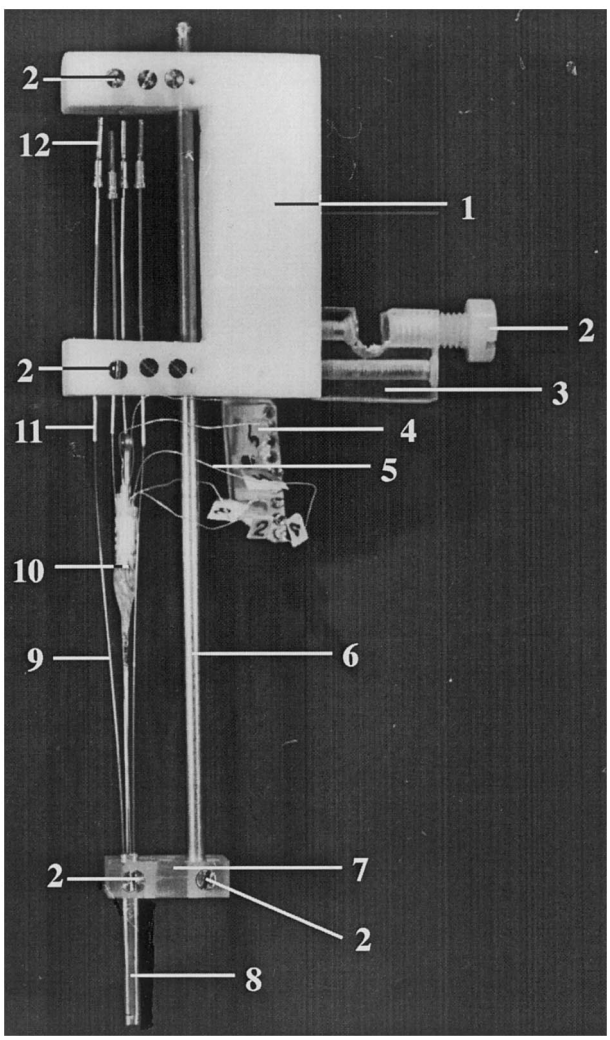

Fig. 1. Microdrive terminal. (1) Teflon fixture; (2) fixation screws; (3) screw clamp for control cable for iontophoresis; (4) pin-mounting board for iontophoretic channels; (5) silver wires; (6) bar for adjusting height; (7) plexiglass guide-holder; (8) electrode guide that contains four polyimide guiding tubes; (9) TE; (10) CE; (11) guiding and electrodefixating tube; (12) connecting tubes for the flexible shafts of the remotely-controlled electrode positioning system.

2.2. General surgical and stereotaxic procedures

Multi-site recordings from different levels of the sensory vibrissal pathway were performed on 31 male Albino Wistar rats (obtained from The Animal Breeding Unit, The Weizmann Institute of Science) that weighed 250–350 g. Within this weight range, the spatial organization (location) of brain structures corresponded to those reported by Paxinos and Watson (1986). Animal maintenance, manipulations, and surgeries were in accordance with institutional animal welfare guidelines, which conform to NIH standards. During the experiments, respiratory complications were prevented by giving each animal atropine methyl nitrate (1 mg/kg, i.m.) prior to general anesthesia. Rats were anesthetized by intraperitoneal administration of urethane (1.5 g/kg), and surgical levels of anesthesia, were maintained by administering 10% of the initial dose of urethane about every 4 h. A local anesthetic, Esracaine (2% solution, 0.5 ml per animal) was used subcutaneously at the site of surgical intervention, and 5% Esracaine ointment was applied to the edges of all surgical wounds. The body temperature of the rats was continuously monitored rectally, and was maintained at ~ 37°C by using a heating pad. The depth of anesthesia was periodically determined by checking the adequacy of respiratory function and the reflexes of eyelids, corneas, and limbs.

Anesthetized rats were mounted on a stereotaxic device (SR-6; Narishige; Tokyo, Japan) using an in-house head-holder without earbars for rats, which is analogous to the device previously described for guinea pigs (Haidarliu, 1996). After removing the scalp and exposing the skull of a rat, separate openings were drilled for cortical, thalamic, and brainstem recordings.

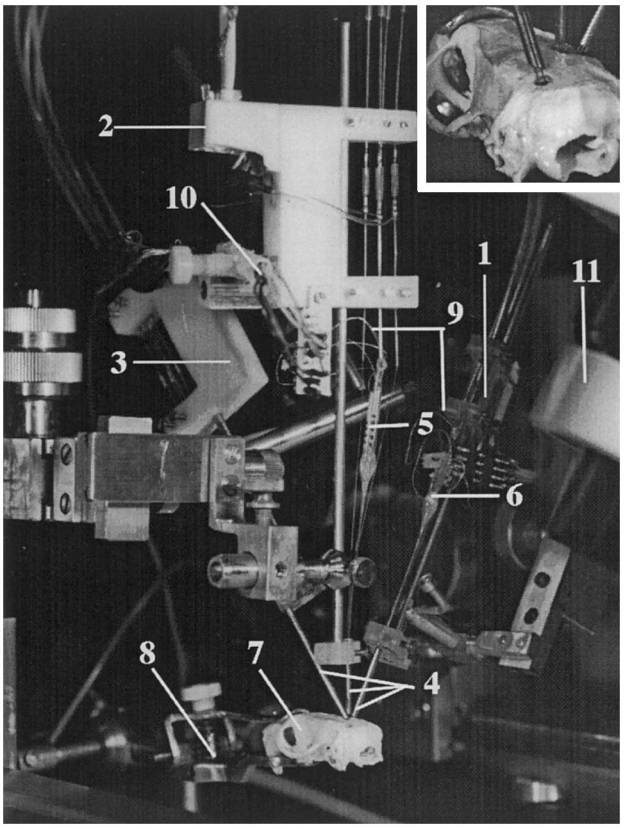

Fig. 2. Arrangement of three remotely-controlled microdrive terminals (1-3) for simultaneous recordings from the cortex (terminal # 1), thalamus (terminal # 2), and brainstem (terminal # 3). Three electrode guides (4), each of which can contain four electrodes [two CEs (5 and 6) for iontophoretic applications to the thalamus (5) and PMBSF (6) are shown], are stereotaxically-oriented relative to the rat skull (7), which is firmly held by a special head-holder without earbars (8). Each iontophoretic capillary of the CEs (5 and 6) is connected via a silver wire (9) to an iontophoretic control cable (10). A binocular microscope (11) is used for the set up of the arrangement. Inset: Close-up of the stereotaxically-positioned electrode guides with electrodes passing through trephanned holes.

For cortical penetrations, an opening was made from 4.5 to 7 mm lateral to the suture sagittalis, and from 1 to 3 mm posterior to the bregma; the dura mater was usually removed from the region that corresponded to the PMBSF. For thalamic penetrations, an opening was made from 1 to 3.5 mm lateral to the suture sagittalis, and from 3 to 5 mm posterior to the bregma; usually, the dura mater was not removed. For penetrations of the trigeminal brainstem nuclei, a trephine hole was made from 2 to 3.5 mm lateral to the midline on the side opposite to the cortical and thalamic openings, and from 7 to 8.5 mm posterior to the bregma; the dura mater was not removed. Drying of the exposed surface of the brain was prevented by constructing a well of dental acrylic that was filled with enough 0.5% agar in physiological saline to cover the distal end of the stainless steel electrode guide.

For cortical recordings, usually a microdrive terminal with a linear configuration of electrodes was used. This configuration permitted placement of all four electrodes along one row of barrels, which was optimal for air-puff stimulations of entire rows. Before each penetration, a picture of the vessel distribution with corresponding coordinates was drawn, and the location of the presumptive PMBSF was estimated. Usually, the PMBSF was located 1.5 to 2.5 mm posterior to the bregma, and 4.5 to 6.5 mm lateral to the midline. Thalamic penetrations were achieved through other holes drilled in the skull, and the electrodes for these penetrations, which were arranged linearly or circularly, were positioned 3.3 to 4.0 mm posterior to the bregma, and 1.6 to 3.0 mm lateral from the midline, and inserted vertically. Brainstem penetrations were achieved through a hole drilled from 7 to 8.5 mm caudal to the bregma. Linear or circular four-electrode arrays were inserted obliquely, in the parasagittal plane, so that the electrodes entered the visual cortex at an angle of 25 to 45 degrees (depending on the targeted nucleus) in the dorso-rostral to ventro-caudal direction (see also Section 4.2).

The major difficulty encountered during simultaneous recordings from the PMBSF, thalamus, and brainstem was that the third micromanipulator, with its microdrive terminal, had to be installed so that it could be moved without interfering with the movements of the other two micromanipulators. This was achieved by constructing a miniature microdrive terminal that was attached independently to the same support bar as one of the other two terminals. The arrangement of all three microdrive terminals for simultaneous recordings from the PMBSF, thalamus, and brainstem is depicted in Fig. 2.

In order to avoid perforation of large blood vessels, penetrations were performed while looking through a binocular microscope. Recording sessions lasted for 10–15 h. At the conclusion of recordings from each electrode penetration, (i) electrolytic lesions were made by passing direct current (3–5 μA in the PMBSF, and 5–8 μA in the thalamus and brainstem) for 4 s at the depth that corresponded to each recorded group of neurons, or (ii) biocytin was ejected from the CEs (50–200 nA, 5 s on/5 s off, for 20–40 min). At the end of the recording session, the animals were euthanized with Pental (1 ml/kg of body weight, i.p.), and perfused transcardially with 0.1 M phosphate buffer (pH 7.4) followed by an ice-cold fixative solution (2.5% glutaraldehyde, 0.5% paraformaldehyde, and 5% sucrose in 0.1 M phosphate buffer, pH 7.4). After perfusion, the brains were removed, separated into blocks of tissue that contained the structures that corresponded to the recorded regions, and postfixed. The postfixed blocks of tissue were cut with a microtome (maintained at tissue-freezing temperatures with dry ice) into thick sections

(50 or 60 μm) that were processed for cytochromoxidase activity (see Haidarliu and Ahissar, 1997), biocytin histochemistry (Horikawa and Armstrong, 1988) and/or Nissl staining.

2.3. Simultaneous recordings from different regions of the central nervous system and microiontophoretic drug applications

We performed concurrent penetrations into up to three of the six structures of the ascending trigeminal pathway: the trigeminal nuclei (principalis, oralis, or interpolaris), the thalamic nuclei (POm or VPM), and the PMBSF. The microdrive terminals (each of which could contain both CEs and TEs) were stereotaxically-oriented, and the electrodes were separately, and independently, advanced to obtain recordings from the PMBSF, thalamic nuclei, and brainstem trigeminal nuclei, as depicted in Fig. 2 (insert). Because of the versatility of our microdrive terminals (which contain independently-movable electrodes), two-site recordings can be achieved with the electrodes in one microdrive terminal, and three-site recordings can be achieved with the electrodes in two microdrive terminals. From each of the electrodes, up to three single- and one multiunit(s) were recorded using commercially-available, digital, template-matching spike sorters (MSD; Alpha Omega Engineering). The local field potential for each electrode was measured with a multi-channel processor (MCP-8000; Alpha Omega Engineering). Iontophoretic applications of acetylcholine (ACh), (1S,3R)-1-aminocyclopentane-1,3-dicarboxylic acid (ACPD), biocytin, carbachol, glutamate, and (S)-α-methyl-4-carboxyphenylglycine (MCPG) (all obtained from Sigma Chemical, Co.; St Louis, MO, USA) were performed with a NeuroPhore BH-2 System (Medical Systems Corp.; Greenvale, NY, USA). The impedance of the glass barrels of the CEs ranged from 10 to 100 MΩ (median of 30 MΩ), depending on the diameter of the orifices of the capillaries and on the solutions with which they were filled. The ejection currents used ranged from 5 to 250 nA (negative currents for ACPD, MCPG and glutamate; positive currents for ACh, carbachol, and biocytin). Retention currents of 5 nA were used to prevent the drugs from leaking when the diameter of the capillary orifices were < 2 μm; retention currents were increased to 8–10 nA when the diameters were 3–4 μm. Balanced ejections were not systematically applied, in order to avoid ejection of the active drug by the balance barrel during retention periods (see Sillito and Kemp, 1983). No qualitative differences were observed between balanced and unbalanced drug applications. At various points along the path of advancement of the electrodes through the structure of interest, spontaneous activity was recorded for 5–10 min, and then followed by different paradigms of vibrissae stimulation (air-puffs or mechanically-provoked vibrations) and iontophoretic drug application.

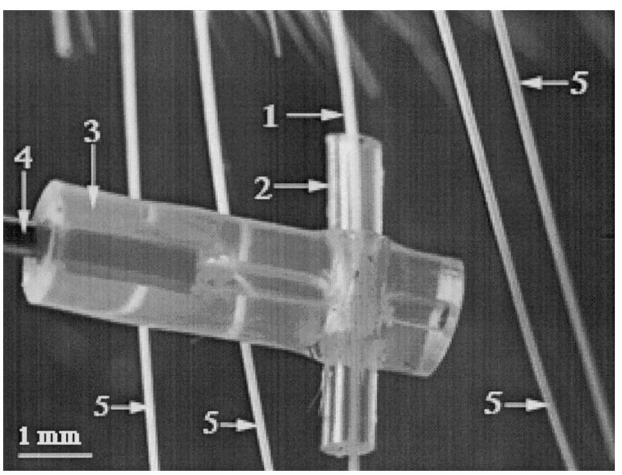

Fig. 3. Mechanical stimulation of a single vibrissa by a vibrating terminal. A vibrissa (1) of the mystacial pad is inserted into a teflon capillary (2) that is inserted perpendicularly through a thicker teflon tube (3). The thicker teflon tube is attached to a vibrating probe (4). The vibrating terminal does not touch neighboring vibrissae (5).

2.4. Tactile stimulations

Mechanical vibrations and pulses of compressed air ('air-puffs') were controlled by the experimental computer. Mechanical vibrations were applied via an electromagnetic linear vibrator (Schneider, 1988), which was attached to a single or several (2–4) vibrissae of a single row. Single vibrissae were inserted into a teflon capillary (inner diameter of 0.4 mm) that was attached to the vibrator (Fig. 3). Multiple vibrissae were attached to a metal spring, which was attached to the vibrator tip. Air-puffs were delivered via a pneumatic pressure pump (Medical Systems; Greenvale, NY), and conducted via a 3 m length of stiff, thick-walled Teflon tubing (6.5 mm OD, 3.5 mm ID). The end of the tubing was narrowed (with a micropipetor tip) to a diameter of 0.7 mm, and was positioned 10–20 mm caudally to the most caudal whiskers of the stimulated rows. Usually, four of the most caudal vibrissae, and their associated straddlers, of one or two neighboring rows of vibrissae were stimulated. The stimuli were delivered as constant pulses; during the first 50 ms of each cycle the whisker was first protracted [(vibrator: rise time = 5 ms, amp = 0.16 mm), (air-puff: rise time = 30 ms, max pressure level at pump output = 0.7 kg/cm^2)] and then retracted (vibrator fall time = 5 ms, air-puff fall time = 10 ms), which produced a constant movement profile for all frequencies. In steady-state experiments, for each frequency, stimuli were applied in trains of 3 or 4 s, where the inter-train intervals were 2 or 1 s, respectively. In frequency modulation experiments, stimuli were applied

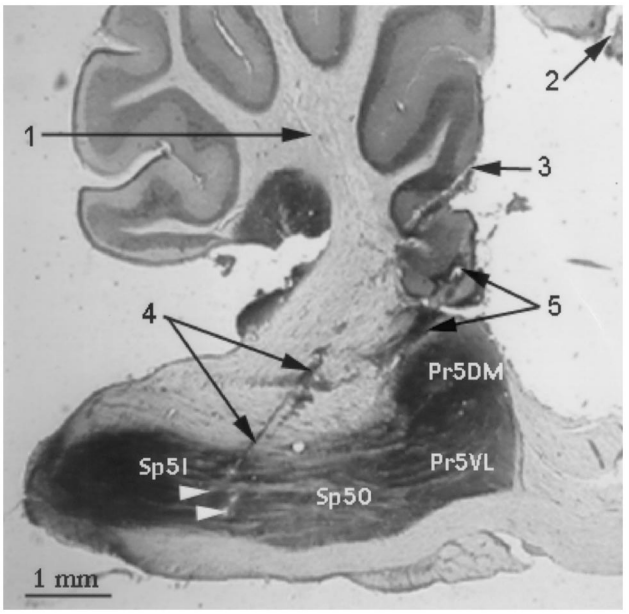

Fig. 4. Penetration into the nucleus interpolaris with two electrodes. This 60 μm thick section was stained for cytochromoxidase activity. (1) cerebellum; (2) electrode track in the visual cortex; (3) electrode track in the anterior part of the cerebellum; (4) two electrode tracks in the inferior cerebellar peduncle and spinal trigeminal tract; (5) tracks of two other electrodes, whose tips were in the Sp50. Arrow heads indicate lesions in the anterior part of the Sp51.

in trains of 8 s with inter-train intervals of 2 s. Air-puff delays (from pump command to whisker movement) were calibrated using a microphone. In all experiments, latencies evoked by air-puffs were compared to those evoked by the mechanical vibrator. In the cases where mismatches (all were < 3 ms) were detected, the mechanical latencies were assumed.

2.5. Data analysis

Data was analyzed for: (i) each neuron separately; (ii) pooled neuronal data from each electrode; and (iii) pooled neuronal data from each recording station. Spike trains were analyzed using laboratory-made software. Peri-stimulus time histograms (PSTHs) were computed using a MATLAB program; computation bin was 1-ms and smoothing consisted of a convolution with a triangle of area 1 and different base lengths. Auto correlograms (ACHs) and cross correlation histograms (CCHs) were computed for each unit and pair of units using a special-purpose C++ program; Computation bins varied between 1 and 10 ms and no smoothing was used. Only analysis of data from well localized recording sites are presented.

3. Results

Our newly-developed system for acute multi-site, multiple-unit recordings and iontophoresis was applied to obtain simultaneous recordings from up to three different stations along the trigeminal pathway. The data presented in this paper were obtained from 31 experiments, in which 207 electrode penetrations into brain tissue were performed. The average number of single-units recorded from a single electrode in a single site was 2.2 ± 0.4, 2.4 ± 0.5, and 2.5 ± 0.5 in the cortex, thalamus, and brainstem, respectively. Since the same electrodes recorded from several sites along the penetration track, the yield per electrode penetration was much higher: 10.5, 8.2, and 7.5 in the cortex, thalamus, and brainstem, respectively. Over all these experiments, 70–80% of the single-units responded to vibrissal stimulations. In addition to the single-units, multi-units and local field potentials were recorded from each electrode.

3.1. Simultaneous recordings from the thalamus and brainstem trigeminal nuclei

Existing surgical procedures for accessing the brainstem trigeminal nuclei entailed either: (i) insertion of electrodes into trigeminal nuclei after the removal of the occipital portion of the skull, part of the cerebellum, and the peduncles of the cerebellum (Klein, 1991; Klein et al., 1998); or (ii) targeting of sensory trigeminal nuclei distantly using stereotaxic coordinates, through small holes made in the skull, usually above the cerebellum (Shipley, 1974). With the first approach, we typically had to resect the dura mater and to excise underlying tissues, which resulted in massive damage to cerebellar tissues and blood vessels. Thermocauterization was usually required to stop the bleeding as a result of damage to blood vessels. We preferred the second approach, in which damage to the tissues and blood vessels was minimal. After trying several different skull sites for the trephine, we concluded that the most suitable were openings drilled according to the coordinates indicated in Section 2. Depending on the nucleus being targeted, the angles chosen for penetration of the electrodes differed: the penetration angles were about 25 degrees for the Pr5, 35 degrees for the Sp50, and 40–45 degrees for the Sp5I and SP5C. An example of a penetration into the nucleus interpolaris is depicted in Fig. 4.

Simultaneous recordings from the brainstem and thalamus are depicted in Fig. 5. Single- and multi-units were recorded from the Sp5I, POm, and VPM during mechanical stimulations of vibrissa E5. The crosscorrelation analysis of these recordings, averaged over 5 stimulating frequencies (2–14 Hz), is summarized in the crosscorrelation matrix (CCM). CCHs describe the probability of a unit to fire as a function of the time-lag

from the triggering event. The CCHs in the left-most column of the CCM were triggered at the onset of the stimulus, and thus, represent the PSTHs of all units. These PSTHs show that most of the units responded sharply to deflection of vibrissae. The other CCHs in the matrix were triggered on different units, and thus, represent inter-neuronal correlations. The CCHs on the main diagonal are correlations of units with themselves, and thus, are called autocorrelation histograms (ACHs). These ACHs provide information about the firing patterns of the different units during stimulation. For example, unit 16, which was recorded from the Sp5I, had a rhythmic firing component at ≈ 25 Hz, which was not correlated with the stimulus. Of the other 28 CCHs, the 16 enclosed by the bold frame demonstrate temporal relationships between brainstem and thalamic neurons. In this example, some of the VPM units (units 1 and 13) fired simultaneously, with no delay, with the Sp5I neurons.

3.2. Simultaneous recordings from the PMBSF and thalamic nuclei

Simultaneous recordings from the PMBSF and both thalamic nuclei (POm and VPM) were performed. An example of such a recording is presented in Fig. 6. Two single-units were recorded from two different electrodes that were inserted into two different locations in layer 5: one underneath a barrel of row D (top row) and one underneath a barrel of row E (second row). Five single-units and two multi-units were recorded from two different electrodes inserted into two different locations

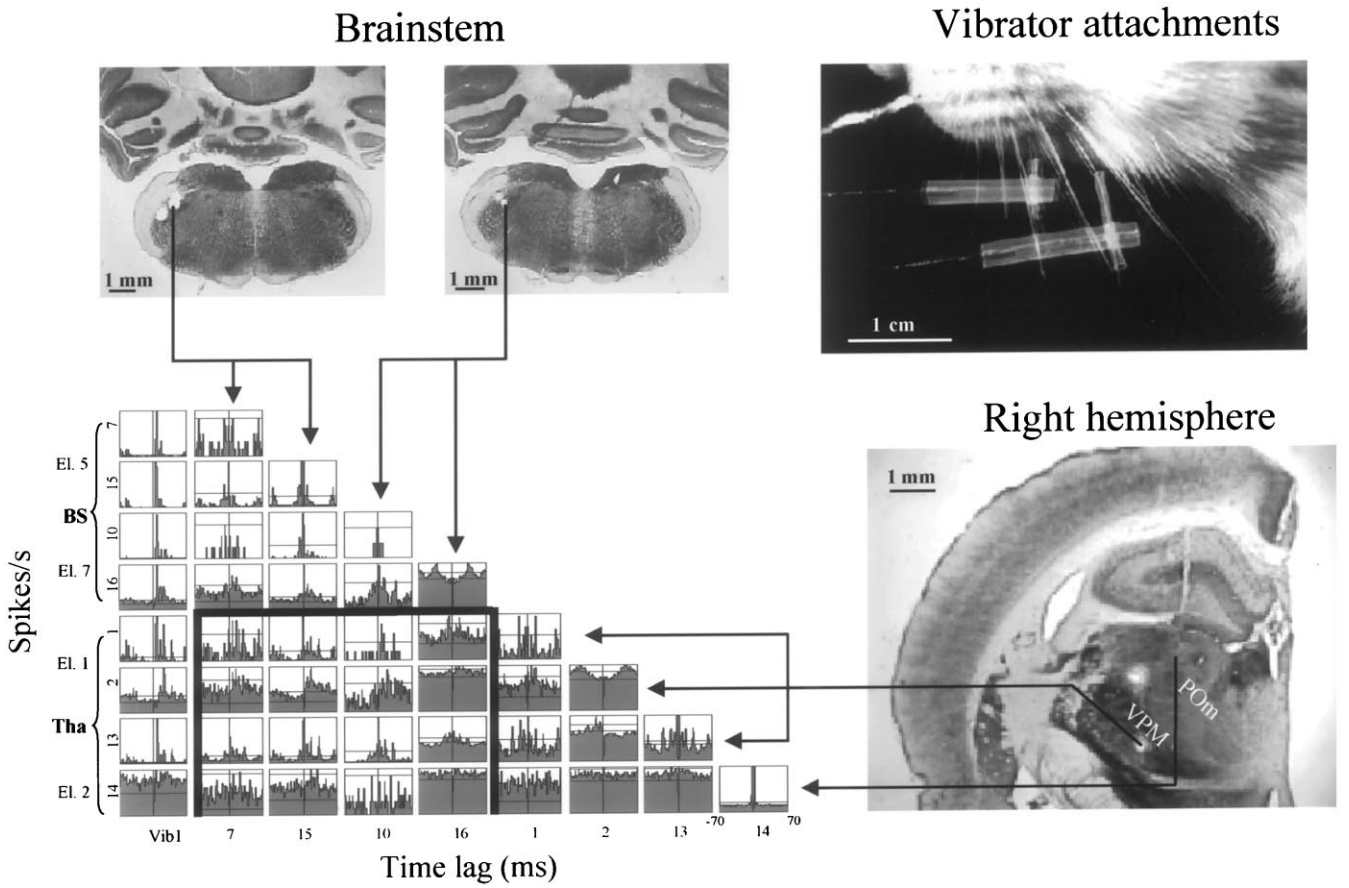

Fig. 5. Simultaneous three-site recordings from the brainstem and two thalamic nuclei (POm and VPM) during stimulation of a single vibrissa. The brainstem units shown were recorded by two (electrodes El. 5 and El. 7) of four electrodes from one microdrive terminal, located in the left SP5I of the brainstem. The lesions produced through these electrodes are indicated on the two histological sections (top panels), which were distanced from each other by about 300 μm antero-posteriorly (left section (2) was more anterior). The thalamic neurons (1)were recorded by two of four electrodes, one located in the right POm of the thalamus (El. 2) and the other in the right VPM (El. 1), of another microdrive terminal. The recording sites of the electrodes were visualized by lesioning and staining of tissue sections for cytochromoxidase activity. Mechanical stimulations of the vibrissae were applied by two mechanical vibrators that were attached to T-shaped probes into which single whiskers were inserted. In this example, only vibrissa E4 was stimulated at 2, 5, 8,11, and 14 Hz: 10-ms protraction of 0.16 mm, 5 mm from the skin. A matrix of all pair-wise CCHs between all recorded units (numerals) and the stimulus (Vib1) is shown. For the PSTHs (left column), maximal firing rates were (top to bottom): 25, 89, 6,107, 23, 66, 457, and 12 spikes/s. Units 7, 10, 1, and 2 were single-units; units 15, 16, 13, and 14 were multi-units. The principal diagonal includes all autocorrelograms. Bin size = 2-ms; time-lag range = −70 to 70-ms; y axis is firing rate, whose scale is independent for each CCH. The CCHs enclosed in the bold frame represent brainstem to thalamus correlations.

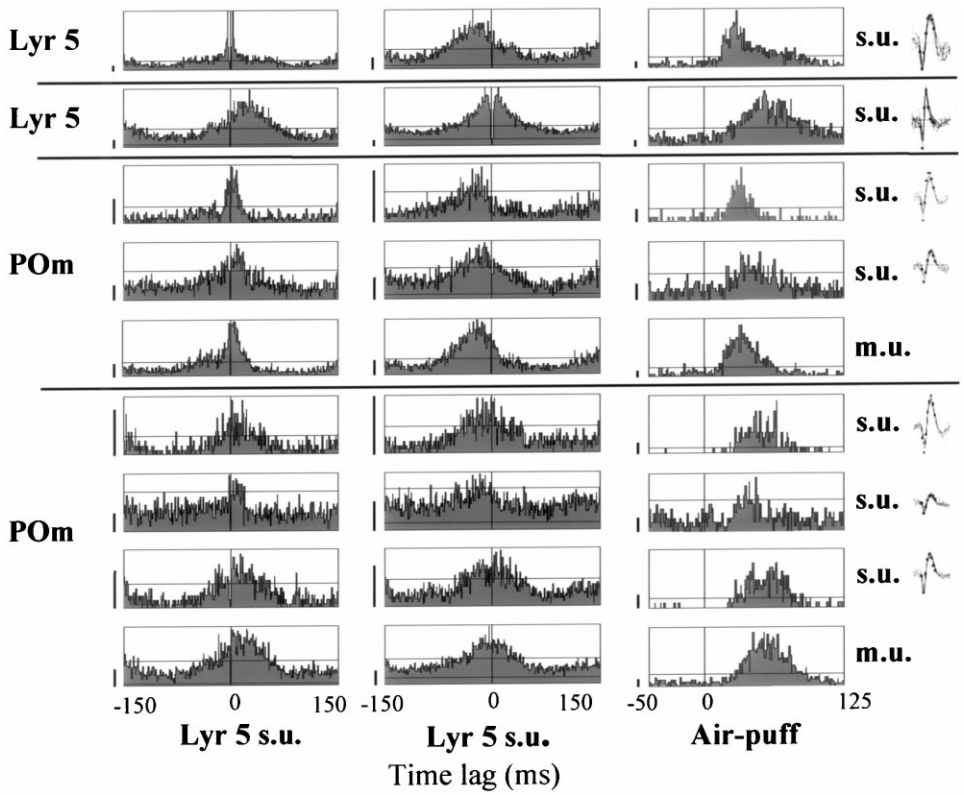

Fig. 6. Simultaneous recordings from the PMBSF and POm during an air-puff stimulation. Recordings from two of the four electrodes that penetrated the cortex and two of the four that penetrated the thalamus are depicted. Stimulus was 50-ms protraction by air-puffs at 5 Hz (24 trains of 3-s + 2-s pause). The locations from which each electrode was recorded are presented on the left. CCHs between two cortical single-units (s.u.) and all recorded units (left and middle columns) and PSTHs (right column) are shown. Time bin = 1-ms. Scale bars on the left of each CCH represent 10 spikes/s. Horizontal lines inside the CCHs indicate significance levels of $P = 0.01$ per bin, assuming independent Poisson processes. Spike shapes of the recorded s.u.s are depicted on the right. Their peak-to-peak amplitudes were (from top to bottom): 248, 351, 163, 110, 496, 150, and 316 μV. The bold dots indicate the templates used for sorting. Signal durations were 2-ms.

in the POm. Rows E and D of the vibrissae were stimulated simultaneously by air-puffs at 5 Hz. The PSTHs (right column) show that the different units responded with different delays to the air-puff stimulations. The exact order of activation is depicted by the CCHs (left and middle columns), which were triggered on the two cortical units. In this example, one unit (left column) phase-led all POm units, while the other cortical unit (middle column), phase-lagged most of the POm units.

3.3. Diffusion in the brain of iontophoretically-ejected biocytin

Biocytin was applied through our CEs during and after the recording of single cortical units. In 4 out of 4 cases, continuous biocytin-stained tissues were limited to < 100 microns from the tip of the electrode. In one representative case (Fig. 7), the electrode track ended at the upper part of layer 5b, where a single pyramidal neuron was stained. The body of this neuron was outside the continuous region of biocytin staining (droplet-stained dark spot; left panel), which demonstrates the limits of diffusion of sufficient biocytin concentrations for visualization by histochemical methods. The diameter of the region of biocytin diffusion in the intercellular space, perpendicular to the electrode penetration axis, was about 80 μm. After supplementary staining with cresyl violet, many cell bodies appeared to be visible at the same distance or even closer to the point of biocytin ejection. Some cell bodies also became visible in the region of biocytin diffusion.

3.4. Simultaneous iontophoretic drug application and extracellular recordings from near and remote sites

Metabotropic glutamate receptors (mGluRs) are involved in the mediation of corticothalamic modulation of thalamocortical transmission (McCormick and von Krosigk, 1992; Eaton and Salt, 1996; Sherman and Guillery, 1996). It was postulated that blocking mGluRs in the thalamus can switch thalamocortical neurons from a hyperpolarized, sensitive mode to a more depolarized, and less-sensitive, 'gating' mode in which their outputs depend on cortical activity (i.e. 'closing' the thalamocortical loop). Thus, local applica-

tions of mGluRs agonists and antagonists should reduce and increase, respectively, thalamic responsiveness. Using our CEs, we were able to apply ACPD, a group I and II mGluR agonist (Salt and Eaton, 1995), and MCPG, a group I and 11 mGluR antagonist (Salt and Turner, 1998), iontophoretically to the vicinity of extracellularly-recorded single- and multi-units in the POm, while recording simultaneously from additional thalamic and cortical electrodes. In preliminary experiments, with air-puff stimulations at 8 Hz, MCPG increased, whereas ACPD decreased, neuronal responsiveness of near (i.e. recorded from the CE) single-units (Fig. 8). Both phasic (immediately following each) and tonic (in between repetitive whisker deflections) components of the response were modulated by these drug applications. The effects were not always consistent across different neurons (Fig. 8). The near m.u. showed a similar pattern, but a reduced effect of MCPG, which might be partially a result of a larger average distance from the electrode tip of the neurons recorded as m.u., and a larger minimal effective concentration required for MCPG compared to ACPD (Holmes et al., 1996). The 'far m.u.', recorded from a different POm electrode (≈ 400 mm away), showed similar response to MCPG but inverted response to ACPD. As expected, the simultaneously recorded cortical m.u. (cx m.u.), was not affected by the thalamic ejection of MCPG. Surprisingly, the thalamic ejection of ACPD increased cortical responsiveness in this particular case.

4. Discussion

The study of neuronal transformations of sensory signals requires recording simultaneously from different levels along sensory pathways. Since these transformations depend on the pharmacological micro-environment of the neurons, methods to control this microenvironment, or to modulate it, are essential. As we demonstrate herein, in the vibrissal system, multi-site recordings, concurrent with local iontophoresis, can be performed simultaneously, with minimal damage to the brain, from the PMBSF in the somatosensory cortex, from the POm and VPM in the thalamus, and from one or more of the four trigeminal subnuclei at the level of the medulla oblongata. Since multi-site recordings can be more traumatic to an organism than single-site recordings, various surgical approaches and electrode tracks were examined, and the least traumatic one chosen. Using this multi-site system we were able to record simultaneously at different levels along the trigeminal pathway while manipulating the pharmacological micro-environment in some of them. This approach enables a comprehensive study of neuronal transfer functions along the sensory pathways.

4.1. Accessibility of recording sites: comparison with previous approaches

Recording from sites that correspond to the same vibrissa is advantageous for understanding the decoding of information encoded during vibrissal touch. In the barrel cortex, we observed that the location of

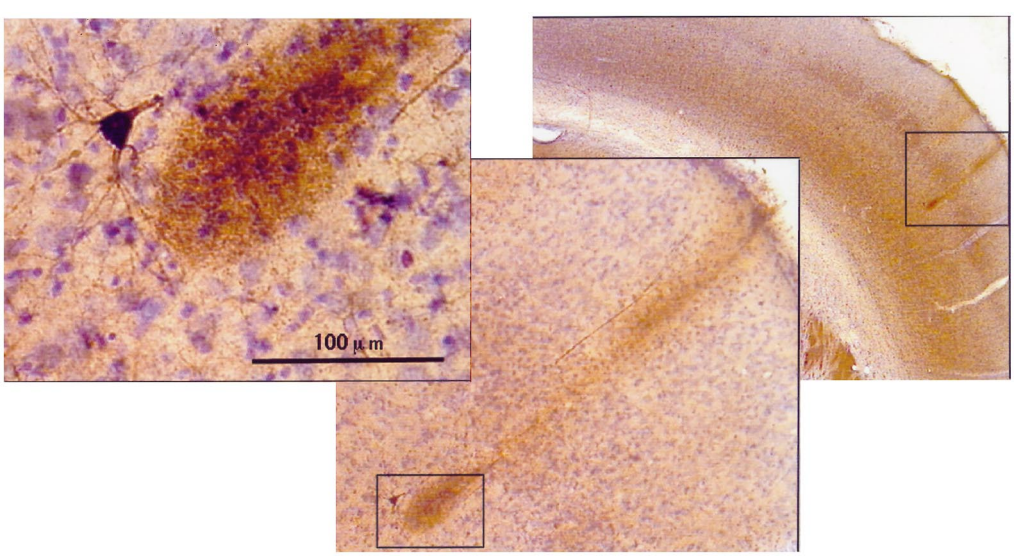

Fig. 7. Staining of a coronal section of the rat brain upon iontophoretic application of biocytin to the upper layer 5b of the PMBSF. Biocytin was ejected (+ 200 nA) for 20 min (non-continuous ejection: 5 s on and 5 s off, total period of 40 min). Sections were processed for biocytin histochemistry and then stained with cresyl violet. The region of biocytin diffusion in the cortex was about 80 μm in diameter. Close to the tip, the diameter of the combined electrode was 25 μm.

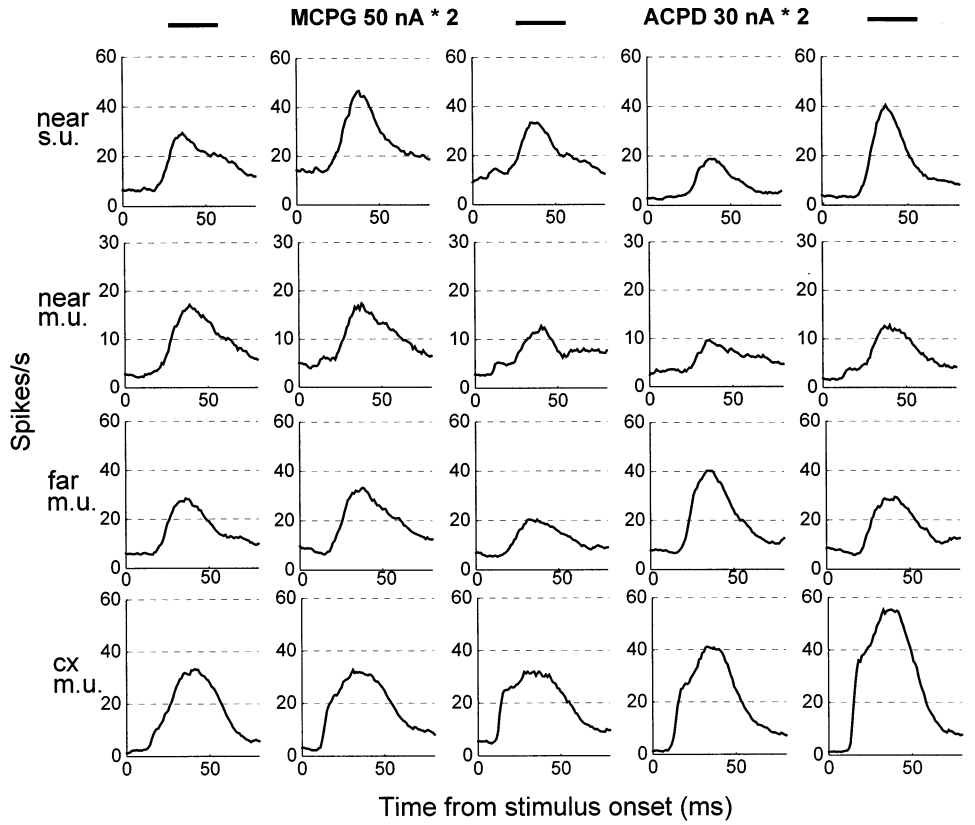

Fig. 8. Effects of iontophoretic applications of MCPG and ACPD in the POm on evoked activity. One single-unit (s.u.) and multi-unit (m.u.) were recorded from the ejecting electrode ('near'). Multi-units were recorded simultaneously from another POm electrode (distanced ≈ 400 μm) and from a cortical electrode (layer 5a). PSTHs of the recorded units, before, during, and after applications of drugs are depicted (bin = 1-ms, smoothed by convolution with a triangle of area 1 and a base of 20-ms to each side). Stimulus was 20-ms protraction pulses by air-puff at 8 Hz (24 trains of 3-s each + 2-s pause; time 0 denotes onset of a stimulus pulse). Drugs [MCPG (50 nA per capillary) or ACPD (30 nA per capillary)] were each applied simultaneously from two of the six CE capillaries of the CE during the entire stimulation period.

individual barrels can be determined with a high degree of probability, even if only one electrode is used. If only one electrode is used in the thalamus, the probability is lower, but can be increased by using an array of four linearly-arranged electrodes, as was used herein. When such electrodes are oriented coronally, they can penetrate into thalamic nuclei (especially the VPM) through all the rows of barreloids, in a consecutive manner starting from the most dorsal row (row A).

In the rat, depending on the site of electrode penetration and location of the targeted nucleus, the distance to the trigeminal nuclei is 8–12 mm from the surface of the brain. Since the vibrissal trigeminal nuclei are located under other structures of the central nervous system, stereotaxic orientation of the electrodes to these nuclei is more complicated than to other structures of the vibrissal pathway. This probably accounts for the variety of surgical approaches previously developed for accessing the brainstem structures. In most of these approaches, overlying tissues are removed in order to reach the trigeminal nuclei. For example, in one approach, the caudal medulla is exposed by removing the overlying part of the skull, the crus II of the cerebellum, and a part of the ventroposteromedial thalamus (Klein, 1991; Klein et al., 1998). In another approach, the caudal medulla and first cervical segment are exposed by laterally retracting the dura and removing most of occipital bone, the pia and arachnoid mater are also removed, and the exposed neural tissues are covered with warm mineral oil (Jacquin et al., 1986).

A direct approach using stereotaxic coordinates, in which the subnucleus Sp5C is first visualized and the obex is used as a reference point, was also used to penetrate the Pr5 and Sp5I (Peschanski, 1984). In approaches where the cerebellum is left intact, penetration into trigeminal nuclei is achieved by inserting electrodes at different angles in relation to the vertical plane (Shipley, 1974; Shortland et al., 1995). Rhoades et al. (1987) used two approaches to penetrate trigeminal nuclei: stereotaxic penetration of the Sp5I and Pr5, and direct penetration into the Sp5I and Pr5 after removal of the muscles and dura overlying the medulla and first cervical segment of the spinal cord. For recording from the nucleus oralis, penetration into the brain stem lateral to the midline between frontal planes was recommended (Dallel et al., 1990).

In our approach for reaching the brainstem trigeminal nuclei, the damage to the brain tissues was minimal. The rat brain was penetrated obliquely (Section 2) at the visual cortex with an array composed of four electrodes. After crossing the visual cortex, the track of the electrodes continued through the anterior part of the cerebellum, the inferior cerebellar peduncle, and the trigeminal tract. The electrodes entered into the trigeminal nuclei starting at the barrelettes of row E, the most dorsal row of barrelettes in these nuclei (see Fig. 4). The arrangement of electrodes in the guide that was positioned parallel to the coronal suture was usually linear. Such an arrangement of the electrodes usually facilitated targeting of brainstem trigeminal nuclei with three of the four electrodes.

When a circular arrangement of electrodes was used for brainstem recordings, good recordings were usually obtained from two or three electrodes, and in some cases, even from all four electrodes. However, with both the linear and circular arrangements of electrodes, the length of the electrode tracks from the surface of the visual cortex to the same row of barrelettes in different nuclei differed for each of the electrodes, because anatomically these structures form angles to the horizontal plane, which vary depending on their distance from the bregma. This variability is seen in the parasagittal sections of the brainstem in the atlas of the rat brain (Paxinos and Watson, 1986), and in Fig. 4 (note the horizontal stripes, which represent the rows of barrelettes, in trigeminal nuclei).

4.2. Targeting of the brainstem nuclei

In all our preparations, the spatial relationships within the brainstem trigeminal nuclei of the rat corresponded to those depicted in the atlas of Paxinos and Watson (1986). However, the spatial relationships between the medulla oblongata and the rest of the brain did not. For successful in vivo targeting of brainstem trigeminal nuclei (from openings on the skull from 7 to 8.5 mm posterior to bregma), we used angles for electrode penetration that were 5 to 8 degrees less than those that would be chosen according to the coordinates in the atlas. This difference in the angles of penetration could be because of slight changes in the properties of tissues during fixation and/or during mounting of sections. The fixation and mounting procedures probably change the position of the medulla oblongata relative to the rest of the brain. Such distortions can easily occur in parasagittal sections that are cut ~ 3 mm lateral to the midline, because at this distance from the midline, the medulla oblongata and anterior part of the brain are interconnected by only a thin bridge of tissue that is composed mainly of white matter, and therefore, cannot maintain their original spatial relationships.

4.3. The order of multi-site penetrations

Since a penetration into the trigeminal nuclei is more complicated and time-consuming than penetrations into the thalamus and cortex, we first penetrated the brainstem nuclei, and located therein groups of cells to be recorded. The next penetration was to the thalamic domains that correspond to the same receptive fields determined for the brainstem. The third penetration was the cortical one, because localization of individual barrels is relatively easy in the somatosensory cortex. Individual barrels in the PMBSF can be mapped in vivo according to the location of the blood vessels that penetrate each barrel. Previously, a similar, but post mortem attempt to locate the vibrissal area according to vascular outlines was undertaken in flattened preparations of mouse and rat cortices by Strominger and Woolsey (1987). Recently, positions of barrels were determined by using a vascular pattern, which was visible through skulls thinned with dental burrs, as a reference (Kim and Ebner, 1999). We were also able to guide cortical penetrations using vascular patterns. Another method that should facilitate cortical localization is intrinsic signal imaging (Grinvald et al. 1986; Frostig, 1994). However, in our experiments, the most reliable indicator for the location of barrels appeared to be the receptive field of an electrode after it had penetrated into the PMBSF. If the electrode happened to shift from the desired location, its position could be rapidly adjusted according to the receptive fields of the first cortical penetration.

4.4. Diffusion of iontophoretically-ejected compounds

The main factor that determines the distribution of iontophorectically-ejected compounds in the brain is diffusion (Curtis et al., 1960). Therefore, the effective concentrations of most iontophoretically applied drugs are limited to a few hundred microns around the tip of the ejecting electrode (Nicholson and Phillips, 1981; Stone, 1985; Nicholson, 1985; Hupe et al., 1999). Previously, we found that the effectiveness of carbachol and ACh drops significantly at distances above 300 μm (Shulz et al., 1997; Haidarliu and Ahissar, unpublished results).

The extent of diffusion in a cell culture can be assessed and visualized by iontophoresis of neuronal markers, such as biocytin (Le and Musil, 1998). Therefore, we used iontophoresis of biocytin as a tool for visually estimating drug diffusion in the brain. The extent of biocytin-stained tissue was less than expected from our cholinergic data (Shulz et al., 1997) and from the data of Hupe et al. (1999) with γ-aminobutyric acid (GABA). The shape of the region of biocytin diffusion appeared to be ellipsoidal (Fig. 7), rather than spherical, as would be expected according to the data of

Hupe et al. (1999). Nevertheless, estimations of the extent of diffusion of biocytin, ACh, and GABA are of the same order of magnitude. Once transport numbers, diffusion coefficients, and minimal effective concentrations are available for all these compounds, better estimations of the extent of diffusion of iontophoretically-applied compounds will be possible.

Iontophoretic applications of modulators of mGluRs should be instrumental in elucidating neuronal processing of sensory information that involves thalamocortical loops. The potential of our system for multi-site recording and iontophoresis in studying the role of mGluRs in the regulation of thalamocortical transfer functions was demonstrated here in preliminary experiments that examined one aspect of tactile responsiveness, the average response to a single deflection pulse during repetitive stimulation. With whisker stimulation at 8 Hz, our data suggest that activation of mGluRs reduces the average response strengths of nearby neurons. This is consistent with the finding that mGluR-mediated activation moves thalamocortical neurons into a gating mode (McCormick and von Krosigk, 1992; Sherman and Guillery, 1996), in which their responses depend on cortical co-activity. Additional experiments are necessary to reveal the involvement of mGluR in the control of thalamocortical transfer functions; for example, the effect of stimulus frequency and the dynamics of response stabilization should be systematically studied. A significant advantage of our system for studying thalamocortical transfer functions is the ability to monitor, simultaneously, the activity of the two major inputs to the thalamocortical neurons (in the cortex and brainstem) and the output activity at the thalamus, and, at the same time, to manipulate and control the pharmacological micro-environment at the vicinity of the recorded thalamic neurons. With this system, most of the major factors that determine thalamic response can be monitored and controlled.

4.5. Advantages of the multi-site recording and iontophoresis system

The most important advantage of our novel system for multi-site recordings over other reported systems is the ability to iontophoretically eject different neuroactive substances simultaneously with extracellular recordings of neuronal activity from multiple sites in the brain. The combination of iontophoresis and multi-site recording enables, for the first time, comprehensive investigations of neuronal transfer functions that involve both neuronal and pharmacological factors. This can be achieved by recording at the input, intermediate, and output levels, while modulating pharmacologically the intermediate level, as demonstrated herein for the thalamocortical vibrissal system.

Another advantage of this recording-ejecting system is its flexibility, which is a result of: (i) the long, stiff, but thin, shafts of the CEs; (ii) the similarity, in shape and treatment, between CEs and regular TEs; (iii) easy attachment of the microdrive terminal to any multichannel electrode advancing system via flexible shafts; (iv) the ability to vary the spatial arrangement of the electrode-directing polyimide tubings inside the stainless steel electrode guides; and (v) being able to use miniature microdrive terminals which allows access to all brain regions (see Fig. 2).

Attachment of each microdrive terminal to the micromanipulators of the stereotaxic device by a 3 mm thick stainless steel bar permits fine tuning of the position of the microdrive terminal and of the angle of electrode penetration. This allows minimizing interference between the different microdrive terminals. This design facilitated our development of a new surgical approach for recordings from brainstem trigeminal nuclei with minimal interference with the thalamic and cortical simultaneous penetrations.

With this new system there is a high probability of targeting neuronal structures located deep in the brain. This advantage was demonstrated by targeting the trigeminal nuclei of the brainstem and the two somatosensory thalamic nuclei, POm and VPM (Figs. 4 and 5), which was possible because of the length and flexibility of the electrodes, and the ability to vary the spatial organization of each electrode array. This versatility of the array was demonstrated by using two different arrangements: linear and circular. Other arrangements can be easily obtained by different arrangements of the polyimid tubings within the electrode guides.

As a result of the independent movement of each electrode, the yield of neuronal recording was significantly better than that achieved with static electrode arrays. In fact, the average number of single-units recorded from our electrodes from a single site was at least twice that reported for static, chronically-implanted arrays (e.g. Nicolelis et al., 1997). Moreover, when the number of single-units recorded along entire penetrations are considered, the yield in our system is about eight times the average yield with static electrodes.

Acknowledgements

We wish to thank Dr. B. Schick for her helpful comments and Yan Karklin for assisting with the figures. This work was supported in part by the Bi-national US-Israel Foundation, Grant # 97-00222 and the MINERVA Foundation (Germany). S.H. was supported by The Center for Absorption in Science, Ministry of Absorption, Israel.

References

Abeles M, Bergman H, Margalit E, Vaadia E. Spatiotemporal firing patterns in the frontal cortex of behaving monkeys. J Neurophysiol 1993;70:1629–38.

Ahissar E. Temporal-code to rate-code conversion by neuronal phase-locked loops. Neural Computations 1998;10:597–650.

Ahissar E, Abeles M, Ahissar M, Haidarliu S, Vaadia E. Hebbian-like functional plasticity in the auditory cortex of the behaving monkey. Neuropharmacol 1998;37:633–55.

Ahissar E, Haidarliu S, Zacksenhouse M. Decoding temporally encoded sensory input by cortical oscillations and thalamic phase comparators. Proc Natl Acad Sci USA 1997;94:11633–8.

Arvidson J. Somatotopic organization of vibrissae afferents in the trigeminal sensory nuclei of the rat studied by transganglionic transport of HRP. J Comp Neurol 1982;211:84–92.

Belford GR, Killackey HP. Vibrissae representation in subcortical trigeminal centers of the neonatal rat. J Comp Neurol 1979;183:305–22.

Carvell GE, Simons DJ. Biometric analyses of vibrissal tactile discrimination in the rat. J Neurosci 1990;10:2638–48.

Curtis DR, Perrin D, Watkin JC. The excitation of spinal neurones by the iontophoretic application of agents which chelate calcium. J Neurochem 1960;6:1–20.

Dallel R, Raboisson P, Woda A, Sessle BJ. Properties of nociceptive and nonnociceptive neurons in trigeminal subnucleus oralis of the rat. Brain Res 1990;521:95–106.

Drake KL, Wise KD, Farraye J, Anderson DJ, BeMent SL. Performance of planar multisite microprobes in recording extracellular single-unit intracortical activity. IEEE Trans Biomed Eng 1988;35:719–32.

Eaton SA, Salt TE. Role of N-methyl-D-aspartate and metabotropic glutamate receptors in corticothalamic excitatory postsynaptic potentials in vivo. Neurosci 1996;73:1–5.

Eichenbaum H, Pettijohn D, Deluca AM, Chorover SL. Compact miniature microelectrode-telemetry system. Physiol Behav 1977;18:1175–8.

Frostig RD. The use of in vivo intrinsic signal imaging for visualization of the functional organization of the brain. Neuroprotocols 1994;5:35–41.

Grinvald A, Lieke E, Frostig RD, Gilbert CD, Wiesel TN. Functional architecture of cortex revealed by optical imaging of intrinsic signals. Nature Lond 1986;324:361–4.

Haidarliu S. An anatomically adapted, injury-free headholder for guinea pigs. Physiol Behav 1996;60:111–4.

Haidarliu S, Ahissar E. Spatial organization of facial vibrissae and cortical barrels in the guinea pig and golden hamster. J Comp Neurol 1997;385:515–27.

Haidarliu S, Shulz D, Ahissar E. A multi-electrode array for combined microiontophoresis and multiple single-unit recordings. J Neurosci Methods 1995;56:125–31.

Holmes KH, Keele NB, Arvanov VL, Shinnick-Gallagher P. Metabotropic glutamate receptor agonist-induced hyperpolarizations in rat basolateral amygdala neurons: receptor characterization and ion channels. J Neurophysiol 1996;76:3059–69.

Horikawa K, Armstrong WE. A versatile means of intracellular labeling: injection of biocytin and its detection with avidin conjugates. J Neurosci Methods 1988;25:1–11.

Hupe J-M, Chouvet G, Bullier J. Spatial and temporal parameters of cortical inactivation by GABA. J Neurosci Methods 1999;86:129–43.

Jacquin MF, Renehan WE, Mooney RD, Rhoades RW. Structure function relationships in rat medullary and cervical dorsal horns: I: trigeminal primary afferents. J Neurophysioi 1986;55:1153–86.

Jellema T, Weijnen JAWM. A slim needle-shaped multiwire microelectrode for intracerebral recording. J Neurosci Methods 1991;40:203–9.

Kim U, Ebner FF. Barrels and septa: separate circuits in rat barrel field cortex. J Comp Neurol 1999;408:489–505.

Klein BG. Chronic functional consequences of adult infraorbital nerve transection for rat trigeminal suboucleus interpolaris. Somatosens Mot Res 1991;8:175–91.

Klein BG, White CF, Duffin JR. Rapid shifts in receptive fields of cells in trigeminal subnucleus interpolaris following infraorbital nerve transection in adult rats. Brain Res 1998;779:136–48.

Kloprogge MJGM. A connector skull cap for neurophysiological studies. Electroenceph Clin Neurophysiol 1971;31:282–3.

Kruger J, Aiple F. Microelectrode investigation of monkey striate cortex: spike train correlations in the infragranular layers. J Neurophysiol 1988;60:798–828.

Kruger J, Bach M. Simultaneous recording with 30 microelectrodes in monkey visual cortex. Exp Brain Res 1981;41:191–4.

Land PW, Buffer SAA, Yaskosky JD. Barreloids in adult rat thalamus: three-dimensional architecture and relationship to somatosensory cortical barrels. J Compar Neurol 1995;355:573–88.

Le A-C, Musil LS. Normal differentiation of cultured lens cells after inhibition of gap junction-mediated intercellula communication. Dev Biol 1998;204:80–96.

Legendy CR, Salcman M, Brennan N. A multiple floating microelectrode for chronic implantation and long-term single unit recording in the cat. Electroenceph Clin Neurophysiol 1984;58:285–8.

Ma PM. The barrelettes-architectonic vibrissal representations in the brainstem trigeminal complex of the mouse: I: normal structural organization. J Comp Neurol 1991;309:161–99.

Ma PM, Woolsey TA. Cytoarchitectonic correlates of the vibrissae in the medullary trigeminal complex of the mouse. Brain Res 1984;306:374–9.

McCormick DA, von Krosigk M. Corticothalamic activation modulates thalamic firing through glutamate metabotropic receptors. Proc Natn Acad Sci USA 1992;89:2774–8.

Mountcastle VB, Reitboeck HJ, Poggio GF, Steinmetz MA. Adaptation of the Reitboeck method of multiple microelectrode recording to the neocortex of the waking monkey. J Neurosci Methods 1991;36:77–84.

Nicholson C. Diffusion from an injected volume of a substance in brain tissue with arbitrary volume fraction and tortuosity. Brain Res 1985;333:325–9.

Nicholson C, Phillips JM. Ion diffusion modified by tortuosity and volume fraction in the extracellular environment of the rat cerebellum. J Physiol Lond 1981;321:225–57.

Nicolelis MAL, Baccala LA, Lin RCS, Chapin JK. Sensorimotor encoding by synchronous neural ensemble activity at multiple levels of the somatosensory system. Science 1995;268:1353–8.

Nicolelis MAL, Ghazanfar M, Faggin BM, Votaw S, Oliveira LMO. Reconstructing the engram: simultaneous, multisite, many single neuron recordings. Neuron 1997;18:529–37.

Nicolelis MAL, Stambaugh CR, Brisben A, Laubach M. Methods for simultaneous multisite neural ensemble recordings in behaving primates. In: Nicolelis MAL, editor. Methods for neural ensemble recordings. Boca Raton: CRC Methods in Neuroscience Series CRC Press, 1999:121–56.

Nordhausen CT, Rousche PJ, Normann RA. Optimizing recording capabilities of the Utah Intracortical Electrode Array. Brain Res 1994;637:27–36.

Olds ME. Enhanced dopamine metabolism in accumbens leads to motor activity and concurrently to increased output from nondopamine neurons in ventral segmental area and substantia nigra. Physiol Behav 1991;51:39–50.

Palmer CL. Long term recordings in the cat motor cortex: unit activity and field potentials from sensory and brain stem stimulation as a means of identifying electrode position. J Neurosci Methods 1990;31:163–81.

Paxinos G, Watson C. The Rat Brain in Stereotaxic Coordinates, second ed. San Diego: Academic Press, 1986.

Peschanski M. Trigeminal afferents to the diencephalon in the rat. Neurosci 1984;12:465–87.

Prut Y, Vaadia E, Bergman H, Haalman I, Slovin H, Abeles M. Spatiotemporal structure of cortical activity: properties and behavioral relevance. J Neurophysiol 1998;79:2857–74.

Reitboeck HJ, Werner G. Multi-electrode recording system for the study of spatiotemporal activity patterns of neurons in the central nervous system. Experimentia 1983;39:339–41.

Rhoades RW, Belford GR, Killackey HP. Receptive-field properties of rat ventral posterior medial neurons before and after selective kainic acid lesions of the trigeminal brain stem complex. J Neurophysiol 1987;57:1577–600.

Salt TE, Eaton SA. Modulation of sensory neurone excitatory and inhibitory responses in the ventrobasal thalamus by activation of metabotropic excitatory amino acid receptors. Neuropharmacol 1995;34:1043–51.

Salt TE, Turner JP. Reduction of sensory and metabotropic glutamate receptor responses in the thalamus by the novel metabotropic glutamate receptor-1 selective antagonist S-2-methyl-4-carboxy-phenylglycine. Neurosci 1998;85:655–8.

Schmidt EM. Electrodes for many single neuron recordings. In: Nicolelis MAL, editor. Methods for Neural Ensemble Recordings. Boca Raton: CRC Press, 1999:1–23.

Schneider W. The tactile array stimulator. John Hopkins APL Technical Digest 1988;9:39–43

Sherman SM, Guillery RW. Functional organization of thalamocortical relays. J Neurophysiol 1996;76:1367–95.

Shipley MT. Response characteristics of single units in the rat's trigeminal nuclei to vibrissa displacements. J Neurophysiol 1974;37:73–90.

Shortland PJ, Jacquin MF, DeMaro JA, Kwan CL, Hu JW, Sessle BJ. Central projections of identified trigeminal primary afferents after molar pulp deafferentation in adult rats. Somatosens Mot Res 1995;12:277–97.

Shulz DE, Cohen S, Haidarliu S, Ahissar E. Differential effects of acetylcholine on neuronal activity and interactions in the auditory cortex of the guinea-pig. Eur J Neurosci 1997;9:396–409.

Sillito AM, Kemp JA. Cholinergic modulation of the functional organization of the cat visual cortex. Brain Res 1983;289:143–55.

Stone TW. Microiontophoresis and Pressure Ejection. New York: John Wiley & Sons, 1985.

Strominger RN, Woolsey TA. Templates for locating the whisker area in fresh flattened mouse and rat cortex. J Neurosci Methods 1987;22:113–8.

Vaadia E, Haalman I, Abeles M, Bergman H, Prut Y, Slovin H, et al. Dynamics of neuronal interactions in monkey cortex in relation to behavioural events. Nature 1995;373:515–8.

Van der Loos H. Barreloids in mouse somatosensory thalamus. Neurosci Lett 1976;2:16.

Van der Loos H. The development of topological equivalences in the brain. In: Meisami E, Brazier MAB, editors. Neural Growth and Differentiation. New York: Raven Press, 1979:331–6.

Villa AEP, Tetko IV, Dutoit P, De Ribaupierre Y, De Ribaupierre F. Corticofugal modulation of functional connectivity within the auditory thalamus of rat, guinea pig and cat revealed by cooling deactivation. J Neurosci Methods 1999;86:161–78.

Vincent SB. The function of the vibrissae in the behavior of the white rat. Behav Monographs 1912;1, no.5, Watson JB ed. Boston:Holt.

Welker WL. Analysis of sniffing of the albino rat. Behavior 1964;22:223–44.

Wiener SL. Spatial and behavioral correlates of striatal neurons in rats performing a selfinitiated navigation task. J Neurosci 1993;13:3802–17.

Woolsey T, Van der Loos H. The structural organization of layer IV in the somatosensory region (Sl) of mouse cerebral cortex: the description of a cortical field composed of discrete cytoarchitectonic units. Brain Res 1970;17:205–42.